13

Rough surfaces

13.1 Real and apparent contact

It has been tacitly assumed so far in this book that the surfaces of contacting bodies are topographically smooth; that the actual surfaces follow precisely the gently curving nominal profiles discussed in Chapters 1 and 4. In consequence contact between them is continuous within the nominal contact area and absent outside it. In reality such circumstances are extremely rare. Mica can be cleaved along atomic planes to give an atomically smooth surface and two such surfaces have been used to obtain perfect contact under laboratory conditions. The asperities on the surface of very compliant solids such as soft rubber, if sufficiently small, may be squashed flat elastically by the contact pressure, so that perfect contact is obtained throughout the nominal contact area. In general, however, contact between solid surfaces is discontinuous and the *real* area of contact is a small fraction of the *nominal* contact area. Nor is it easy to flatten initially rough surfaces by plastic deformation of the asperities. For example the serrations produced by a lathe tool in the nominally flat ends of a ductile compression specimen will be crushed plastically by the hard flat platens of the testing machine. They will behave like plastic wedges (§6.2(*c*)) and deform plastically at a contact pressure $\approx 3Y$ where Y is the yield strength of the material. The specimen as a whole will yield in bulk at a nominal pressure of Y. Hence the maximum ratio of the real area of contact between the platen and the specimen to the nominal area is about $\frac{1}{3}$. Strain hardening of the crushed asperities will decrease this ratio further.

We are concerned in this chapter with the effect of surface roughness and discontinuous contact on the results of conventional contact theory which have been derived on the basis of smooth surface profiles in continuous contact.

Most real surfaces, for example those produced by grinding, are not regular: the heights and the wavelengths of the surface asperities vary in a random way.

A machined surface as produced by a lathe has a regular structure associated with the depth of cut and feed rate, but the heights of the ridges will still show some statistical variation. Most man-made surfaces such as those produced by grinding or machining have a pronounced 'lay', which may be modelled to a first approximation by one-dimensional roughness. It is not easy to produce a wholly isotropic roughness. The usual procedure for experimental purposes is to air-blast a metal surface with a cloud of fine particles, in the manner of shot-peening, which gives rise to a randomly cratered surface. Before discussing random rough surfaces, however, we shall consider the contact of regular wavy surfaces.

The simplest model of a rough surface is a regular wavy surface which has a sinusoidal profile. Provided that the amplitude Δ is small compared with the wavelength λ so that the deformation remains elastic, the contact of such a surface with an elastic half-space can be analysed by the methods of Chapters 2 and 3.

13.2 Contact of regular wavy surfaces

(a) One-dimensional wavy surface

We will start by considering an elastic half-space subjected to a sinusoidal surface traction

$$p = p^* \cos(2\pi x/\lambda) \tag{13.1}$$

which alternately pushes the surface down and pulls it up. The normal displacements of the surface under this traction can be found by substituting (13.1) into equation (2.25*b*), i.e.

$$\frac{\partial \bar{u}_z}{\partial x} = -\frac{2(1-\nu^2)}{\pi E}\int_{-\infty}^{\infty} \frac{p^* \cos(2\pi s/\lambda)}{x-s}\,\mathrm{d}s$$

$$= -\frac{2(1-\nu^2)}{\pi E}\, p^* \int_{-\infty}^{\infty} \frac{\cos\{2\pi(x-\xi)/\lambda\}}{\xi}\,\mathrm{d}\xi$$

Expanding the numerator and integrating gives

$$\frac{\partial \bar{u}_z}{\partial x} = -\frac{2(1-\nu^2)}{E}\, p^* \sin(2\pi x/\lambda) \tag{13.2}$$

or

$$\bar{u}_z = \frac{(1-\nu^2)\lambda}{\pi E}\, p^* \cos(2\pi x/\lambda) + \text{const.} \tag{13.3}$$

Not surprisingly the sinusoidal variation in traction produces a sinusoidal surface of the same wavelength.

https://doi.org/10.1017/CBO9781139171731.014 Published online by Cambridge University Press

The stresses within the solid may be found by superposition of the stresses under a line load (eq. (2.23)) or, more directly, by equations (2.6) from the stress function

$$\phi(x, z) = (p^*/\alpha^2)(1 + \alpha z)\, e^{-\alpha z} \cos \alpha x \tag{13.4}$$

where $\alpha = 2\pi/\lambda$. The maximum principal shear stress τ_1 occurs at a depth $z = \lambda/2\pi$ beneath the points of maximum traction ($x = n\pi$). Its value is p^*/e.

If an elastic half-space with a flat surface is brought into contact with an elastic solid, whose nominally flat surface before loading has a one-dimensional wave of small amplitude Δ and wavelength λ, the gap between the surfaces may be expressed by† (see Fig. 13.1(*a*))

$$h(x) = \Delta\{1 - \cos(2\pi x/\lambda)\} \tag{13.5}$$

If the surfaces are now pressed into contact by a mean pressure $\bar{p}$ sufficient to compress the wave completely so that the surfaces are in continuous contact, the pressure distribution can be found from the above results. The elastic displacements of the surfaces are such that

$$(\bar{u}_z)_1 + (\bar{u}_z)_2 = \delta - h(x) \tag{13.6}$$

where δ is the approach of datum points in each body. Equation (13.3) shows that this equation is satisfied by a pressure distribution of the form

$$p(x) = \bar{p} + p^* \cos(2\pi x/\lambda) \tag{13.7}$$

where $p^* = \pi E^* \Delta/\lambda$, since the uniform pressure $\bar{p}$ produces a uniform displacement. For contact to be continuous the pressure must be positive everywhere so that $\bar{p} \geqslant p^*$ (see Fig. 13.1(*b*)).

If the mean pressure is less than p^* there will not be continuous contact between the two surfaces. They will make contact in parallel strips of width $2a$ located at the crests of the undulations and will separate in the troughs (see Fig. 13.1(*c*)). Westergaard (1939) has shown that a pressure distribution:

$$p(x) = \frac{2\bar{p}\cos(\pi x/\lambda)}{\sin^2(\pi a/\lambda)} \{\sin^2(\pi a/\lambda) - \sin^2(\pi x/\lambda)\}^{1/2} \tag{13.8}$$

acting on an elastic half-space produces normal surface displacements:

$$\bar{u}_z(x) = \frac{(1 - \nu^2)\bar{p}\lambda}{\pi E \sin^2 \psi_a} \cos 2\psi + C, \quad 0 \leqslant |x| \leqslant a \tag{13.9a}$$

† The same form of expression for the undeformed gap is obtained if *both* surfaces have parallel undulations of the same wavelength, even though the undulations are displaced in phase so that initial contact does not occur at the crests.

$$\bar{u}_z(x) = \frac{(1-\nu^2)\bar{p}\lambda}{\pi E \sin^2 \psi_a}\left[\cos 2\psi + 2\sin\psi\,(\sin^2\psi - \sin^2\psi_a)^{1/2} - 2\sin^2\psi_a \ln\left\{\frac{\sin\psi + (\sin^2\psi - \sin^2\psi_a)^{1/2}}{\sin\psi_a}\right\}\right] + C,$$

$$a \leqslant |x| \leqslant \lambda/2, \tag{13.9b}$$

where $\bar{p}$ is the mean pressure, $\psi = \pi x/\lambda$, $\psi_a = \pi a/\lambda$, and C is a constant determined by the datum chosen for displacements. The displacements of (13.9*a*) satisfy the contact condition (13.6) for $|x| \leqslant a$ provided that

$$\bar{p} = (\pi E^*\Delta/\lambda)\sin^2(\pi a/\lambda) \tag{13.10}$$

and the displacements outside the contact strip ($a \leqslant |x| \leqslant \lambda/2$) are such that the gap remains positive. Noting from equation (13.7) that $(\pi E^*\Delta/\lambda) = p^*$, equation (13.10) can be inverted to express the ratio of the 'real' to the 'apparent' area of contact, i.e.

$$2a/\lambda = (2/\pi)\sin^{-1}(\bar{p}/p^*)^{1/2} \tag{13.11}$$

This relationship is plotted in Fig. 13.2. When $\bar{p} \ll p^*$, then $2a \ll \lambda$, and the compression of the crest of each wave should be independent of the other waves,

Fig. 13.1. Contact of a one-dimensional wavy surface with an elastic half-space. (*a*) Unloaded ($\bar{p} = 0$), (*b*) Complete contact ($\bar{p} = p^*$), (*c*) Partial contact ($\bar{p} < p^*$).

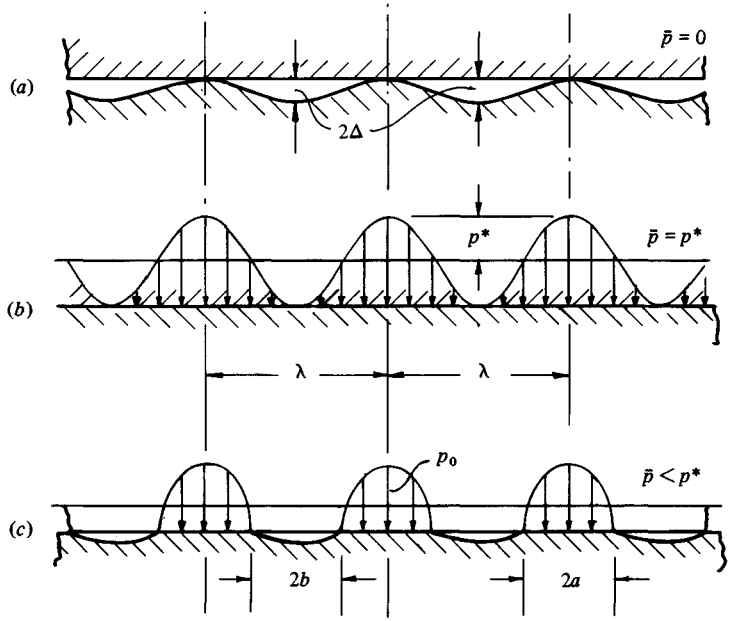

https://doi.org/10.1017/CBO9781139171731.014 Published online by Cambridge University Press

so that the Hertz theory might be applied. The load P carried by each crest is $\bar{p}\lambda$ and the curvature $1/R$ of each crest is $4\pi^2\,\Delta/\lambda^2$. Substituting these values in the Hertz equation (4.43) for line contact gives

$$2a/\lambda = (2/\pi)(\bar{p}/p^*)^{1/2} \tag{13.12}$$

which is the limit of equation (13.11) for $\bar{p} \ll p^*$. It is shown dotted in Fig. 13.2.

At the other limit when $\bar{p} \to p^*$ only a small strip of width $2b$ ($\ll\lambda$) remains out of contact, where $b = \lambda/2 - a$. An asymptotic expression for b can be found by regarding the non-contact zone as a pressurised crack of length $2b$ in an infinite solid. The contact pressure in the non-contact zone is, of course, zero, but it can be thought of as the superposition of the pressure necessary to maintain the surfaces in contact, given by (13.7), and an equal negative pressure acting on the surface of the 'crack' ($a \leqslant x \leqslant \lambda - a$). Provided $b \ll \lambda/2$ the pressure within the crack may be written

$$p(x') \approx 2\pi^2(x'/\lambda)^2 p^* - (p^* - \bar{p}) \tag{13.13}$$

where $x' = x - \lambda/2$. Since the interface has no strength it will open until the stress intensity factor at its ends falls to zero. The stress intensity factor at the ends of a pressurised crack of length $2b$ is given by (see Paris & Sim, 1965)

$$K_I = (\pi b)^{-1/2} \int_{-b}^{b} p(x')\{(b + x')/(b - x')\}^{1/2}\,dx' \tag{13.14}$$

Fig. 13.2. Real area of contact of a one-dimensional wavy surface with an elastic half-space. Solid line – exact, eq. (13.11); broken line – asymptotic, eqs. (13.12) and (13.15).

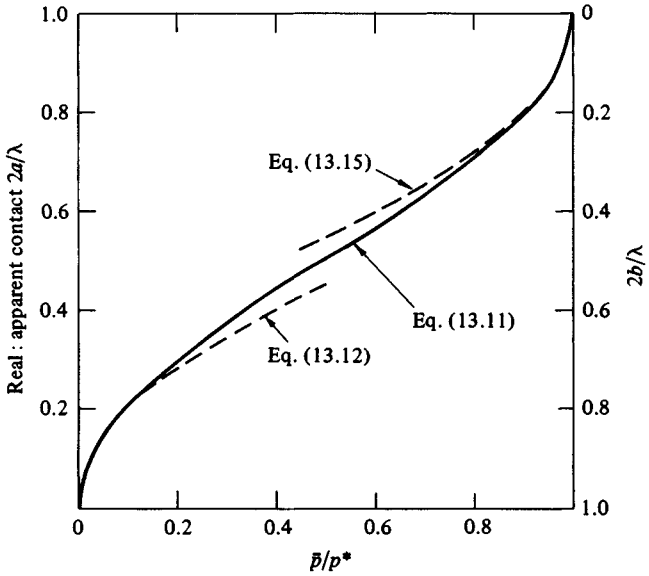

https://doi.org/10.1017/CBO9781139171731.014 Published online by Cambridge University Press

Substituting $p(x')$ from (13.13), integrating and equating K_I to zero give the length of the no-contact zone to be

$$2b/\lambda = (2/\pi)(1 - \bar{p}/p^*)^{1/2} \tag{13.15}$$

which is the limit of equation (13.11) as $\bar{p} \to p^*$. It is also plotted in Fig. 13.2, where it may be seen that the asymptotic equations (13.12) and (13.15) provide close bounds on the exact result. As we shall see below, in the case of a two-dimensional wavy surface, only the asymptotic results can be obtained in closed form.

(b) Two-dimensional waviness

The gap between a flat surface and one which has a regular orthogonal waviness can be expressed by

$$h(x,y) = \Delta_1 + \Delta_2 - \Delta_1 \cos(2\pi x/\lambda_1) - \Delta_2 \cos(2\pi y/\lambda_2) \tag{13.16}$$

The surfaces touch at the corners of a rectangular grid of mesh size $\lambda_1 \times \lambda_2$; the maximum gap, which coincides with a hollow in the surface, has a depth $2(\Delta_1 + \Delta_2)$ at the mid-point of the rectangle. After compression the elastic displacements, in the area over which the surfaces are in contact, are given by substituting (13.16) in (13.6). The pressure to make contact over the whole surface can now be found by superposition of the pressures necessary to compress each of the component waves taken separately. Thus by equation (13.7) we have

$$p(x,y) = \bar{p} + p_x^* \cos(2\pi x/\lambda_1) + p_y^* \cos(2\pi y/\lambda_2) \tag{13.17}$$

where $p_x^* = \pi E^* \Delta_1/\lambda_1$ and $p_y^* = \pi E^* \Delta_2/\lambda_2$. To maintain contact everywhere $\bar{p} \geqslant p_x^* + p_y^*$. When the mean pressure is less than this value the interface will comprise areas of contact and separation. At low pressures the contact area at a crest will be elliptical and given by Hertz theory. At high pressures the small area of separation will also be elliptical and can be found by modelling it as a pressurised crack. In between, the shape of the contact area will not be elliptical and a closed-form solution seems improbable.

For an isotropic wavy surface $\Delta_1 = \Delta_2 = \Delta$, $\lambda_1 = \lambda_2 = \lambda$ whereupon we can write equation (13.17) as

$$p(x,y) = \bar{p} + \tfrac{1}{2}p^* \{\cos(2\pi x/\lambda) + \cos(2\pi y/\lambda)\} \tag{13.18}$$

where $p^* = 2\pi E^* \Delta/\lambda$. The curvature of a peak in the surface $1/R = 4\pi^2 \Delta/\lambda^2$ and the load carried by each peak $P = \bar{p}\lambda^2$. Substituting these values in the Hertz equation (4.22) gives the ratio of the real (circular) area of contact to the nominal (square) area:

$$\frac{\pi a^2}{\lambda^2} = \pi \left(\frac{3}{8\pi} \frac{\bar{p}}{p^*} \right)^{2/3} \tag{13.19}$$

https://doi.org/10.1017/CBO9781139171731.014 Published online by Cambridge University Press

At the other extreme, when contact is nearly complete, the approximately circular region of no-contact is regarded as a 'penny-shaped crack' subjected to an internal pressure equal and opposite to that given by equation (13.18). As before the radius of the crack b is found from the condition that the stress intensity factor at the edge of the crack should be zero. In this way (see Johnson *et al.*, 1985) it is found that

$$\frac{\pi b^2}{\lambda^2} = \frac{3}{2\pi}\left(1 - \frac{\bar{p}}{p^*}\right) \tag{13.20}$$

Both asymptotic results, given by equations (13.19) and (13.20) are plotted in Fig. 13.3. In between, numerical solutions by Johnson *et al.* (1985) show how the ratio of the real to apparent contact area varies with contact pressure. The photographs of a rubber model in Fig. 13.4 illustrate the changing shape of the contact area.

(c) Plastic crushing of a serrated surface

If a regular wavy surface, compressed by a rigid flat die, yields before it is flattened elastically, the crests of the waves will be crushed plastically. It

Fig. 13.3. Real area of contact of a two-dimensional wavy surface with an elastic half-space. Broken line – asymptotic, eqs. (13.19) and (13.20); solid circle – numerical solutions; open circle – experimental from Fig. 13.4.

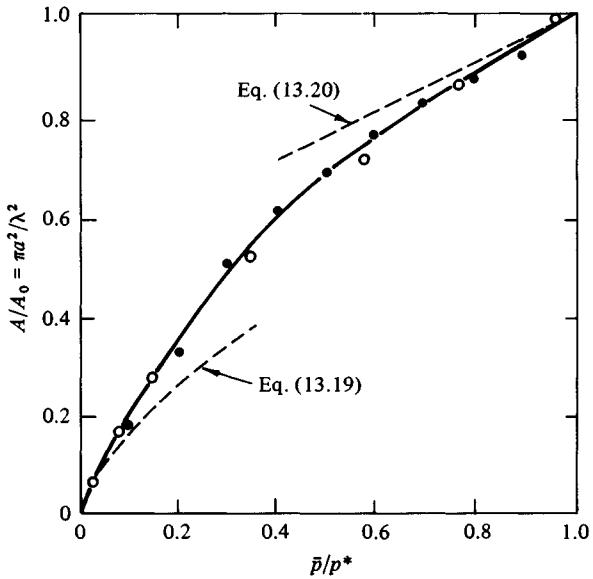

https://doi.org/10.1017/CBO9781139171731.014 Published online by Cambridge University Press

has then been observed that it is difficult to flatten the surface by plastic crushing of the asperities (see Greenwood & Rowe, 1965). This behaviour has been modelled by Childs (1973) by representing the rough surface by a regular array of wedge-shaped serrations, which is indented by a flat rigid punch whose width L is much greater than the pitch of the serrations, as shown in Fig. 13.5(a). When the punch is loaded by a normal force P the tips of the serrations are crushed, each with a contact width l. Taking the material of the serrated surface to be rigid-perfectly-plastic, the serrations will first crush according to the slip-line field of Fig. 6.8(b) from which the asperity pressure p can be calculated. With increasing load, this mode of deformation will continue until the deformation fields of adjacent serrations begin to overlap, i.e. when point C in Fig. 6.8(b) reaches the trough between two serrations. For a semi-wedge-angle $\alpha = 65°$ this point is reached when $l/\lambda = 0.36$. Further deformation is now constrained by the interference between adjacent serrations. Slip-line fields have been constructed by Childs (1973) for this situation which results in a sharp increase in asperity pressure as $l/\lambda \to 1.0$. This configuration may be visualised as a back extrusion, where the material displaced by the downward motion of the punch has to be extruded upwards through the small remaining

Fig. 13.4. Area of contact between a perspex flat and a rubber block with an isotropic wavy surface $\bar{p}/p^*$: (a) 0.024, (b) 0.080, (c) 0.139, (d) 0.345, (e) 0.550, (f) 0.759.

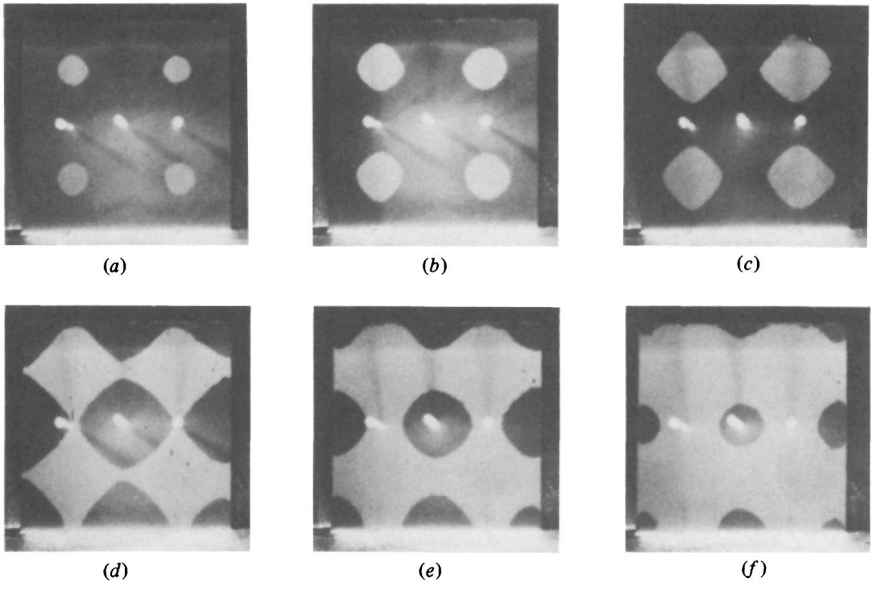

https://doi.org/10.1017/CBO9781139171731.014 Published online by Cambridge University Press

gap between the contact areas. The mean pressure on the punch $\bar{p}$ is given by:

$$\frac{\bar{p}}{2k} \equiv \frac{P}{2kL} \approx \frac{p}{2k}\frac{l}{\lambda} \tag{13.21}$$

When $\bar{p}$ reaches the limiting pressure for plastic indentation of a flat punch (5.14k), the punch will indent the block as a whole and no further deformation of the asperities will take place. In the example shown in Fig. 13.5(b) ($\alpha = 65°$), this limit is reached when $l/\lambda = 0.81$. In practice the asperities strain-harden relative to the bulk so that the maximum value of l/λ is less than 0.81. Thus, under purely normal loading of an extended surface, it is not possible to crush the asperities flat by purely plastic deformation. We have seen that this arises

Fig. 13.5. Crushing a regular serrated plastic surface by a rigid flat punch ($\alpha = 65°$). Bulk indentation by the punch will occur when $pl/\lambda = \bar{p} = P/L = 5.14k$, i.e. when $l/\lambda = 0.81$.

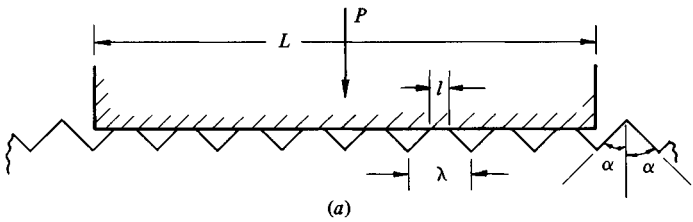

(a)

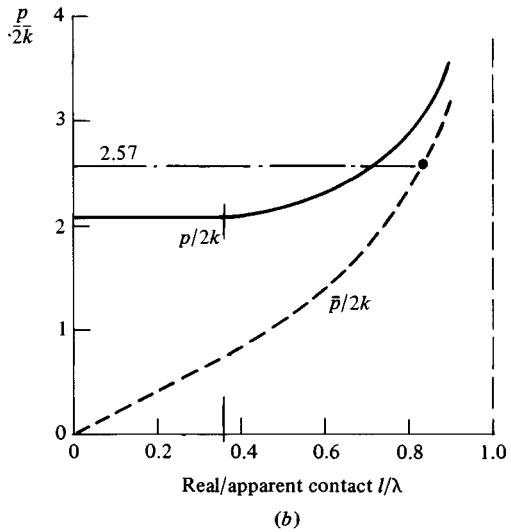

(b)

https://doi.org/10.1017/CBO9781139171731.014 Published online by Cambridge University Press

from the constraint imposed by adjacent asperities. If, however, the block as a whole is extending plastically parallel to the surface of the punch (neglecting friction) this constraint is removed and the asperities are flattened by small punch pressures. This state of affairs is common at the surface of a die in a metal forming operation. It also occurs if the block in Fig. 13.5(*a*) is not as wide as the punch so that bulk plastic flow takes place when $\bar{p}$ exceeds $2k$. Finally, frictional shearing of the serrations by a tangential force applied to the block facilitates the growth of the real/apparent contact area l/λ. The mode of plastic deformation of the serrations is then similar to that of the wedge shown in Fig. 7.15.

13.3 Characteristics of random rough surfaces

We will now discuss briefly the topographical characteristics of random rough surfaces which are relevant to their behaviour when pressed into contact.

Surface texture is most commonly measured by a profilometer which draws a stylus over a sample length of the surface of the component and reproduces a magnified trace of the surface profile as shown in Fig. 13.6. Note that the trace is a much distorted image of the actual profile through using a larger magnification in the normal than in the tangential direction. Modern profilometers digitise the trace at a suitable sampling interval and couple the output to a computer in order to extract statistical information from the data. First, a datum or centre-line is established by finding the straight line (or circular arc in the case of round components) from which the mean square deviation is a minimum. This implies that the area of the trace above the datum is equal to that below it. The average roughness is now defined by

$$R_a \equiv \frac{1}{L}\int_0^L |z|\,dx \tag{13.22}$$

where $z(x)$ is the height of the surface above the datum and L is the sampling length. A less common but statistically more meaningful measure of average roughness is the 'root-mean-square' or standard deviation σ of the height of the

Fig. 13.6. Profilometer trace.

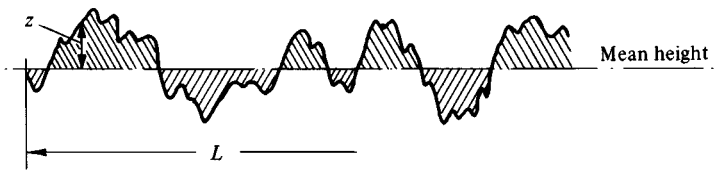

https://doi.org/10.1017/CBO9781139171731.014 Published online by Cambridge University Press

surface from the centre-line, i.e.

$$\sigma^2 = \frac{1}{L}\int_0^L z^2 \, dx \tag{13.23}$$

The relationship between σ and R_a depends, to some extent, on the nature of the surface; for a regular sinusoidal profile $\sigma = (\pi/2\sqrt{2})R_a$, for a Gaussian random profile $\sigma = (\pi/2)^{1/2}R_a$.

The R_a value by itself gives no information about the shape of the surface profile, i.e. about the *distribution* of the deviations from the mean. The first attempt to do this was by the so-called bearing area curve (Abbott & Firestone, 1933). This curve expresses, as a function of height z, the fraction of the nominal area lying within the surface contour at elevation z. It would be obtained from a profile trace, such as Fig. 13.6, by drawing lines parallel to the datum at varying heights z and measuring the fraction of the length of the line at each height which lies within the profile (see Fig. 13.7). We note in passing that the 'bearing area curve' does not give the true bearing area when the rough surface is in contact with a smooth flat one. It implies that the material in the area of interpenetration vanishes, no account being taken of contact deformation. The true bearing or contact area will be discussed in §4.

An alternative approach to the bearing area curve is through elementary statistics. If we denote by $\phi(z)$ the probability that the height of a particular point in the surface will lie between z and $z + dz$, then the probability that the height of a point on the surface is greater than z is given by the cumulative probability function: $\Phi(z) = \int_z^\infty \phi(z')\, dz'$. This yields an S-shaped curve identical with the bearing area curve.

It has been found that many real surfaces, notably freshly ground surfaces, exhibit a height distribution which is close to the 'normal' or Gaussian probability

Fig. 13.7. Height distribution $\phi(z)$ and 'bearing area' curve given by the cumulative height distribution $\Phi(z)$.

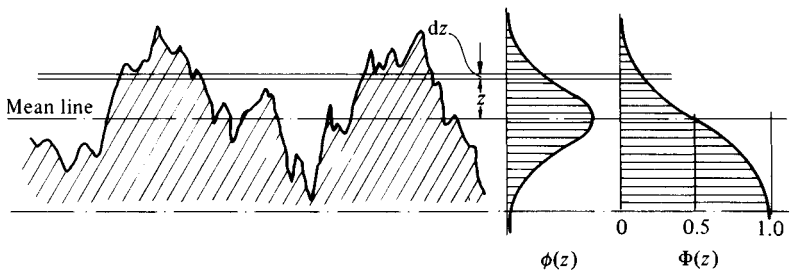

https://doi.org/10.1017/CBO9781139171731.014 Published online by Cambridge University Press

function:

$$\phi(z) = \sigma^{-1}(2\pi)^{-1/2} \exp(-z^2/2\sigma^2) \tag{13.24}$$

where σ is the standard (r.m.s.) deviation from the mean height. The cumulative probability

$$\Phi(z) = \tfrac{1}{2} - \frac{1}{(2\pi)^{1/2}} \int_0^{z/\sigma} \exp(-z'^2/2\sigma^2)\, \mathrm{d}(z'/\sigma) \tag{13.25}$$

is to be found in any statistical tables. When plotted on normal probability graph paper, data which follow the normal or Gaussian distribution will fall on a straight line whose gradient gives a measure of the standard deviation σ, as shown by the ground surface in Fig. 13.8(*a*). It is convenient from a mathematical point of view to use the normal probability function in the analysis of randomly rough surfaces, but it must be kept in mind that few real surfaces are Gaussian. For example, a ground surface which is subsequently polished so that the tips of the higher asperities are removed (Fig. 13.8(*b*)) departs markedly from the straight line in the upper height range. A lathe-turned surface is far from random; its peaks are nearly all the same height and its troughs the same depth. It appears on probability paper as shown in Fig. 13.8(*c*).

So far we have discussed only variations in height of the surface; spatial variations must also be considered. There are several ways in which the spatial variation can be specified. We shall use the root-mean-square slope σ_m and r.m.s. curvature σ_κ defined as follows.†

A sample length L of the surface is traversed by a stylus profilometer and the height z is sampled at discrete intervals of length h. If z_{i-1}, z_i and z_{i+1} are three consecutive heights, the slope is defined by

$$m = (z_{i+1} - z_i)/h \tag{13.26}$$

and the curvature by

$$\kappa = (z_{i+1} - 2z_i + z_{i-1})/h^2 \tag{13.27}$$

The r.m.s. slope and curvature are then found from

$$\sigma_m^2 = (1/n) \sum_{i=1}^{i=n} m^2 \tag{13.28}$$

$$\sigma_\kappa^2 = (1/n) \sum_{i=1}^{i=n} \kappa^2 \tag{13.29}$$

where $n = L/h$ is the total number of heights sampled.

† For alternative specifications of a random rough surface in terms of the *auto-correlation function* or the *spectral density*, the interested reader is referred to the book: *Rough Surfaces*, Ed. T. R. Thomas (1982).

Fig. 13.8. Cumulative height distributions plotted on normal probability paper: solid circle – surface heights; cross – peak heights; triangle – summit heights. (*a*) Bead-blasted aluminium, (*b*) mild steel abraded and polished, (*c*) lathe-turned mild steel (Williamson, 1967–8).

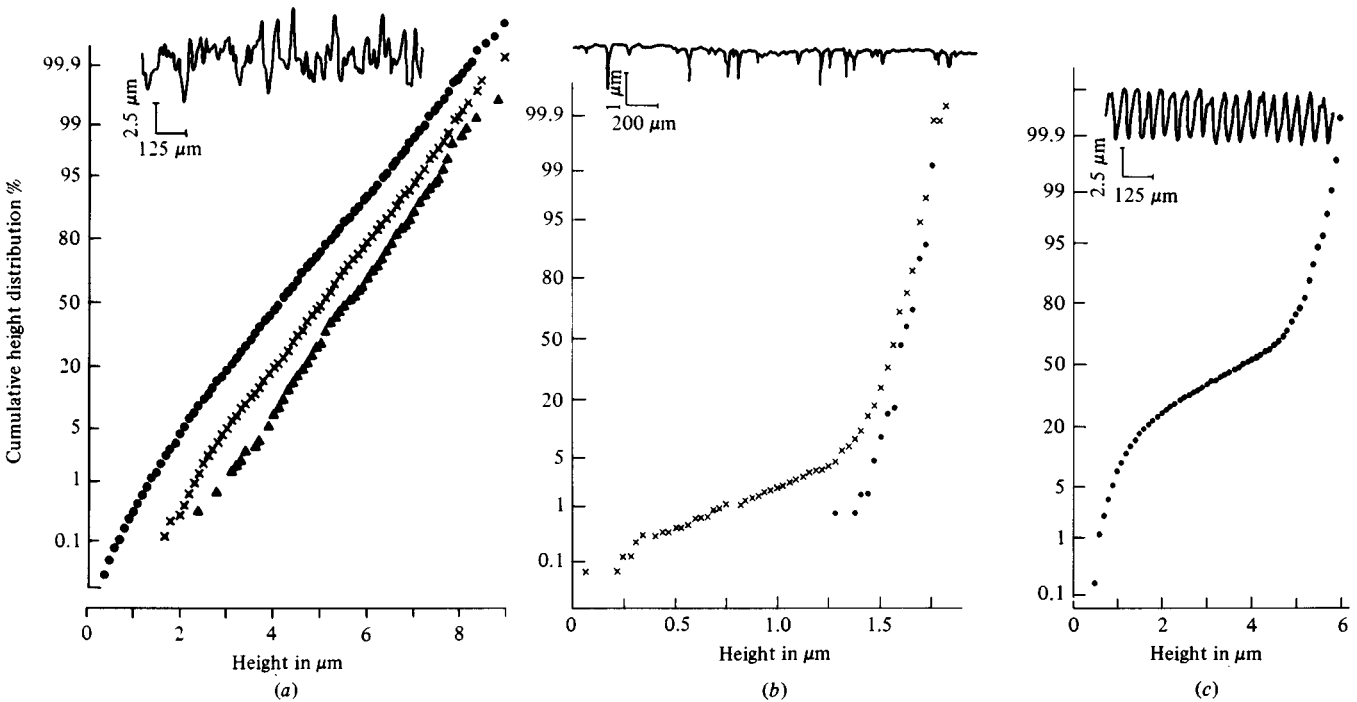

We should like to think of the parameters σ, σ_m and σ_κ as properties of the surface which they describe. Unfortunately their values in practice depend upon both the sample length L and the sampling interval h used in their measurement. If we think of a random rough surface as having a continuous spectrum of wavelengths, neither wavelengths which are longer than the sample length nor those which are shorter than the sampling interval will be recorded faithfully by a profilometer. A practical upper limit for the sample length is imposed by the size of the specimen and a lower limit to the meaningful sampling interval by the radius of the profilometer stylus. The mean square roughness σ is virtually independent of the sampling interval h provided that h is small compared with the sample length L. The parameters σ_m and σ_κ, however, are very sensitive to sampling interval: their values tend to increase without limit as h is made smaller, and shorter and shorter wavelengths are included. This uncomfortable fact has led to the concept of *functional filtering* whereby both the sample length and sampling interval are chosen to be appropriate to the particular application under consideration. We shall return to this point in §5.

When rough surfaces are pressed into contact they touch at the high spots of the two surfaces, which deform to bring more spots into contact. We shall see in the next section that, to quantify this behaviour, we need to know the standard deviation of the asperity heights σ_s, the mean curvature of their summits $\bar{\kappa}_s$, and the asperity density η_s, i.e. the number of asperities per unit area of the surface. These quantities have to be deduced from the information contained in a profilometer trace. It must be kept in mind that a maximum in the profilometer trace, referred to as a 'peak', does not necessarily correspond to a true maximum in the surface, referred to as a 'summit', since the trace is only a one-dimensional section of a two-dimensional surface. On the basis of random process theory, following the work of Longuet-Higgins (1957*a* & *b*), Nayak (1971) and Whitehouse & Phillips (1978, 1982), Greenwood (1984) has investigated the relationship between the summit properties of interest and the properties of a profilometer trace as influenced by sampling interval, with the following conclusions:

(i) For an isotropic surface having a Gaussian height distribution with standard deviation σ, the distribution of summit heights is very nearly Gaussian with a standard deviation

$$\sigma_s \approx \sigma \tag{13.30}$$

The mean height of the summits lies between 0.5σ and 1.5σ above the mean level of the surface. The same result is true for peak heights in a profilometer trace, as shown by the data in Fig. 13.8(*a*), where the fact that the data for the peak heights and summit heights lie approximately parallel to those for the surface as a whole, shows that they have

nearly the same standard deviation. A peak in the profilometer trace is identified when, of three adjacent sample heights, z_{i-1}, z_i and z_{i+1}, the middle one z_i is greater than both the outer two.

(ii) The mean summit curvature is of the same order as the root-mean-square curvature of the surface, i.e.,

$$\bar{\kappa}_s \approx \sigma_\kappa \tag{13.31}$$

(iii) By identifying peaks in the profile trace as explained above, the number of peaks per unit length of trace η_p can be counted. If the wavy surface were regular, as discussed in §2(*b*), the number of summits per unit area η_s would be η_p^2. Nayak (1971) showed that, for a *random* isotropic surface, with a vanishingly small sampling interval, $\eta_s = 1.209\eta_p^2$. Over a wide range of finite sampling intervals Greenwood (1984) showed that

$$\eta_s \approx 1.8\eta_p^2 \tag{13.32}$$

Although the sampling interval has only a second-order effect on the relationships between summit and profile properties expressed in equations (13.31) and (13.32), it must be emphasised that the profile properties themselves σ_κ and η_p are both very sensitive to the size of the sampling interval.

13.4 Contact of nominally flat rough surfaces

We have seen throughout this book that, in the frictionless contact of elastic solids, the contact stresses depend only upon the *relative* profile of their two surfaces, i.e. upon the shape of the gap between them before loading. The system may then be replaced, without loss of generality, by a flat, rigid surface in contact with a body having an effective modulus E^* and a profile which results in the same undeformed gap between the surfaces. We are concerned here with the contact of two nominally flat surfaces, which have r.m.s. roughnesses σ_1 and σ_2 respectively. However we shall consider the contact of a rigid flat plane with a deformable surface of equivalent roughness $\sigma = (\sigma_1^2 + \sigma_2^2)^{1/2}$.

The situation is illustrated in Fig. 13.9. We shall follow the analysis of Greenwood & Williamson (1966). The mean level of the surface is taken as

Fig. 13.9. Contact of a randomly rough surface with a smooth flat.

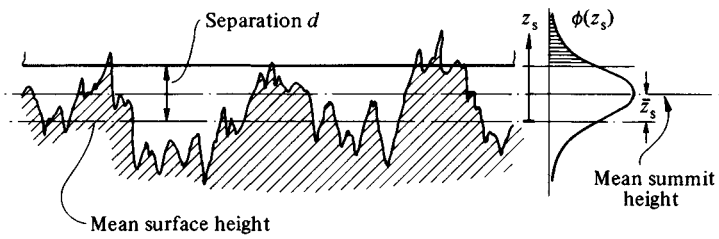

https://doi.org/10.1017/CBO9781139171731.014 Published online by Cambridge University Press

datum and the distance between the datum and the rigid flat is referred to as the separation. Fig. 13.9 shows the peaks in a profile trace but, from the contact point of view we are interested in the summits of the surface asperities. We shall denote the summit heights by z_s, having a mean $\bar{z}_s$ and a distribution function $\phi(z_s)$, which expresses the probability of finding a summit of height z_s lying in the interval z_s to $z_s + dz_s$. If there are N summits in the nominal surface area A_0, the number of summits in contact at a separation d is given by

$$n = N \int_d^\infty \phi(z_s)\, dz_s \tag{13.33}$$

For simplicity we shall follow Greenwood & Williamson (1966) and assume that the asperity summits are spherical with a *constant* curvature κ_s. If a summit height exceeds the separation it will be compressed by $\delta = z_s - d$ and make contact with the flat in a small circular area of radius a. The ith summit, therefore, has a contact area

$$A_i = \pi a_i^2 = f(\delta_i) \tag{13.34}$$

and the force required to compress it may be written

$$P_i = g(\delta_i) \tag{13.35}$$

where the functions $f(\delta)$ and $g(\delta)$ depend upon the material properties of the surfaces. If the deformation is entirely within the elastic limit, from the Hertz equation (4.23),

$$f(\delta) = \pi\delta/\kappa_s \tag{13.36}$$

and

$$g(\delta) = (\tfrac{4}{3})E^*\kappa_s^{-1/2}\delta^{3/2} \tag{13.37}$$

For perfectly plastic compression of an asperity, if 'piling-up' or 'sinking in' is neglected (see §6.3):

$$f(\delta) \approx 2\pi\delta/\kappa_s \tag{13.38}$$

and

$$g(\delta) \approx \bar{p}A \approx 6\pi Y\delta/\kappa_s \tag{13.39}$$

where Y is the yield strength of the softer surface. Halling & Nuri (1975) have proposed alternative functions $f(\delta)$ and $g(\delta)$ appropriate to a material which displays power-law strain hardening.

To find the total real area of contact A and the total nominal pressure $\bar{p}$ $(= P/A_0)$ we must sum equations (13.34) and (13.35) for all the asperities in contact, i.e. those whose height z_s exceeds the separation d. Thus

$$A = N \int_d^\infty f(z_s - d)\phi(z_s)\, dz_s \tag{13.40}$$

https://doi.org/10.1017/CBO9781139171731.014 Published online by Cambridge University Press

and

$$\bar{p}A_0 \equiv P = N\int_d^\infty g(z_s - d)\phi(z_s)\,dz_s \tag{13.41}$$

Greenwood & Williamson (1966) have evaluated these integrals numerically for elastically deforming asperities (eq. (13.36) and (13.37)) and a Gaussian distribution of asperity heights.

The contact area (non-dimensionalised) is plotted against the non-dimensional load in Fig. 13.10 from which it may be seen that the contact area is approximately proportional to the load over three decades of load. The separation may be normalised by subtracting the mean summit height and dividing by the standard deviation, i.e. by putting $\zeta = (d - \bar{z}_s)/\sigma_s$. The theory is based on the assumption that the deformation of each asperity is independent of its neighbours. This will become increasingly in error when the real contact area is no longer small compared with the nominal area, at normalised separations less than 0.5, say. At the other end of the scale, the probability of contact becomes negligible if the normalised separation exceeds about 3.0.

The significant features of Greenwood & Williamson's results may be demonstrated without recourse to numerical analysis by using an exponential rather

Fig. 13.10. Real area of contact of a randomly rough elastic surface with a smooth flat: A – Gaussian distribution of asperity heights (Greenwood & Williamson, 1966); B – exponential distribution (eq. (13.46)).

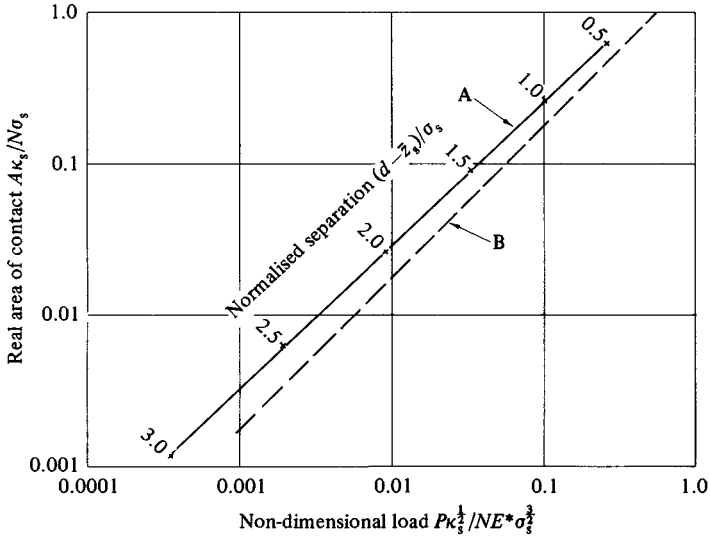

https://doi.org/10.1017/CBO9781139171731.014 Published online by Cambridge University Press

than a Gaussian distribution function, i.e. by putting

$$\phi(z_s) = (C/\sigma_s) \exp(-z_s/\sigma_s), \quad z_s > 0 \tag{13.42}$$

where C is an arbitrary constant. The number of asperities in contact, given by (13.33), then becomes

$$\begin{aligned} n &= (CN/\sigma_s) \int_d^\infty \exp(-z_s/\sigma_s)\, dz_s \\ &= CN \exp(-d/\sigma_s) \int_0^\infty \exp(-\delta/\sigma_s)\, d(\delta/\sigma_s) \\ &= CN \exp(-d/\sigma_s) \end{aligned} \tag{13.43}$$

Similarly equation (13.40) for the contact area becomes

$$\begin{aligned} A &= (CN/\sigma_s) \int_d^\infty f(\delta) \exp(-z_s/\sigma_s)\, dz_s \\ &= CN \exp(-d/\sigma_s) \int_0^\infty f(\delta/\sigma_s) \exp(-\delta/\sigma_s)\, d(\delta/\sigma_s) \\ &\equiv nI_f \end{aligned} \tag{13.44}$$

and equation (13.41) for the load becomes

$$\begin{aligned} P &= CN \exp(-d/\sigma_s) \int_0^\infty g(\delta/\sigma_s) \exp(-\delta/\sigma_s)\, d(\delta/\sigma_s) \\ &\equiv nI_g \end{aligned} \tag{13.45}$$

The definite integrals in equations (13.44) and (13.45), denoted by I_f and I_g respectively, are constants independent of the separation d. Thus the real contact area A and the mean pressure $\bar{p}$ are both proportional to the number of asperities in contact n, and are hence proportional to each other irrespective of the mode of deformation of the asperities expressed by f and g. These results imply that, although the size of each particular contact spot grows as the separation is decreased, the number of spots brought into contact also increases at a rate such that the *average* size $\bar{a}$ remains constant.

If the deformation of the asperities is elastic $f(\delta/\sigma_s)$ and $g(\delta/\sigma_s)$ are given by equations (13.36) and (13.37) which, when substituted in (13.44) and (13.45), give $I_f = \pi\sigma_s/\kappa_s$ and $I_g = \pi^{1/2} E^* \sigma_s^{3/2} \kappa_s^{-1/2}$. Thus the ratio of the real to apparent contact area is given by

$$\frac{A}{A_0} = \frac{A}{P}\frac{P}{A_0} = \frac{I_f}{I_g}\bar{p} = \pi^{1/2}(\sigma_s\kappa_s)^{-1/2}(\bar{p}/E^*) \tag{13.46}$$

where $\bar{p}$ is the nominal contact pressure P/A_0. In this case, with an exponential

https://doi.org/10.1017/CBO9781139171731.014 Published online by Cambridge University Press

probability function, the number of asperities in contact and the real area of contact are both exactly proportional to the load. The comparison with the more realistic Gaussian distribution is shown in Fig. 13.10.

It is instructive to compare the ratio of real to apparent area of contact for a random rough surface, given by equation (13.46), with that for a *regular* wavy surface. Now equation (13.19) for the real area of contact of a flat surface with a regular wavy surface of amplitude Δ may be written

$$A/A_0 = 0.762(\Delta \kappa_s)^{-1/2}(\bar{p}/E^*)^{2/3} \tag{13.47}$$

Recognising that the standard deviation σ of a random rough surface is a comparable quantity to the amplitude Δ of a regular wavy surface, we see that equations (13.46) and (13.47) involve the same dimensionless variables. Whereas the regular surface deforms such that the real area of contact grows as the $(\text{load})^{2/3}$, the contact area with a randomly rough surface grows in direct proportion with the load. This conclusion is consistent with Amontons' law of friction. Frictional forces must be developed at the points of real contact and we would expect, therefore, that the total force of friction would be proportional to the real area of contact, which we have seen is in direct proportion to the load. Further experimental support for the conclusions presented above is provided by measurements of thermal and electrical conductance between conducting bodies across a rough interface. The conductance of a single circular contact area is given by $2Ka$, where K is the bulk conductivity of the solids. The total conductance of the interface therefore is $2K\Sigma a = 2Kn\bar{a}$. Now we have seen that the mean contact size $\bar{a}$ remains approximately constant while the number of contact spots n increases in direct proportion to the load, thereby ensuring that the total conductance increases in proportion to the load. The law of friction demands that the total area (Σa^2) increases in proportion to the nominal contact pressure (load); the conductance experiments demand that Σa increases in direct proportion to load. The only simple way in which both these conditions can be fulfilled simultaneously is by the mean contact *size* $\bar{a}$ remaining constant and the *number* of real contact spots n increasing in proportion to the load.

A further consequence of the area of real contact being proportional to the load is that the real mean contact pressure is nearly constant. For an exponential probability function and elastically deforming asperities,

$$\bar{p}_r = \frac{P}{A} = \frac{I_g}{I_f} = 0.56E^*(\sigma_s\kappa_s)^{1/2} \tag{13.48}$$

For a Gaussian height distribution $\bar{p}_r$ varies from 0.3 to $0.4E^*(\sigma_s\kappa_s)^{1/2}$ over the relevant range of loading. Since each asperity in the model is spherical the onset of plastic yield is given by equation (6.9), i.e. when $\bar{p} = 1.1Y \approx 0.39H$, where

https://doi.org/10.1017/CBO9781139171731.014 Published online by Cambridge University Press

H is the hardness of the material and Y its yield stress. Thus the average contact pressure will be sufficient to cause yield if $\bar{p}_r \geqslant 0.39H$, that is if

$$\psi \equiv (E^*/H)(\sigma_s \kappa_s)^{1/2} \geqslant C \tag{13.49}$$

where C is a constant which depends somewhat on the height distribution but has a value close to unity The non-dimensional parameter ψ is known as the 'plasticity index'. It describes the deformation properties of a rough surface. If its value is appreciably less than unity the deformation of the asperities when in contact with a flat surface will be entirely elastic; if the value exceeds unity the deformation will be predominantly plastic.

The theory outlined above assumes that the asperities have a constant curvature κ_s whereas, in reality, the summit curvatures will have a random variation. As an approximation we can use the mean summit curvature $\bar{\kappa}_s$ in equations (13.44)–(13.49) which, as we saw in the last section (eq. (13.31)), is approximately equal to the r.m.s. curvature of the surface found from a profilometer trace. This procedure is not strictly correct because the summit curvature is not independent of the summit height, but it has been justified by Onions & Archard (1973).

An alternative definition of the plasticity index has been proposed by Mikic (1974). We saw in §6.3 that the extent of plastic deformation during the indentation of an elastic-plastic surface by a rigid wedge or cone was governed by the non-dimensional parameter $(E^* \tan \beta/Y)$ where β is the angle of inclination of the face of the wedge or cone to the surface of the solid and Y is the yield stress. Thus, when two rough surfaces are in contact we might expect the degree of plastic deformation of the asperities to be proportional to the *slope* of the asperities. Remembering that yield stress is proportional to hardness, Mikic proposed a plasticity index defined by

$$\psi = E^* \sigma_m / H \tag{13.50}$$

where σ_m is the r.m.s. slope of the surface which is obtained directly from a profile trace. This definition avoids the difficulty of two statistical quantities which are not independent, but does not escape the dependence of σ_m on the sampling interval used to measure it.

13.5 Elastic contact of rough curved surfaces

We come now to the main question posed in this chapter: how are the elastic contact stresses and deformation between curved surfaces in contact, which form the main subject of this book, influenced by surface roughness? The qualitative behaviour is clear from what has been said already. There are two scales of size in the problem: (i) the bulk (nominal) contact dimensions and elastic compression which would be calculated by the Hertz theory for the

'smooth' mean profiles of the two surfaces and (ii) the height and spatial distribution of the asperities. For the situation to be amenable to quantitative analysis these two scales of size should be very different. In other words, there should be many asperities lying within the nominal contact area. When the two bodies are pressed together true contact occurs only at the tips of the asperities, which are compressed in the manner discussed in §4. At any point in the nominal contact area the nominal pressure increases with overall load and the real contact area increases in proportion; the average real contact pressure remains constant at a value given by equation (13.48) for elastically deforming asperities. Points of real contact with the tips of the higher asperities will be found outside the nominal contact area, just as a rough seabed results in a ragged coastline with fjords and off-shore islands. The asperities act like a compliant layer on the surface of the body, so that contact is extended over a larger area than it would be if the surfaces were smooth and, in consequence, the contact pressure for a given load will be reduced. Quantitative analysis of these effects, using the Greenwood & Williamson model of a rough surface (spherically tipped elastic asperities of constant curvature), has been applied to the point contact of spheres by Greenwood & Tripp (1967) and Mikic (1974) and to the line contact of cylinders by Lo (1969). We shall consider the axi-symmetric case which can be simplified to the contact of a smooth sphere of radius R with a nominally flat rough surface having a standard distribution of summit heights σ_s, where R and σ_s are related to the radii and roughnesses of the two surfaces by: $1/R = 1/R_1 + 1/R_2$ and $\sigma_s^2 = \sigma_{s1}^2 + \sigma_{s2}^2$.

Referring to Fig. 13.11, a datum is taken at the mean level of the rough surface. The profile of the undeformed sphere relative to the datum is given by

$$y = y_0 - r^2/2R$$

At any radius the combined normal displacement of both surfaces is made up of a bulk displacement w_b and an asperity displacement w_a. The 'separation' d between the two surfaces contains only the bulk deformation, i.e.

$$d(r) = w_b(r) - y(r) = -y_0 + (r^2/2R) + w_b(r) \tag{13.51}$$

The asperity displacement $w_a = z_s - d$, where z_s is the height of the asperity summit above the datum. If now we assume that the asperities deform elastically, the function $g(w_a)$ is given by equation (13.37) with δ replaced by w_a. Then, by substitution in equation (13.41), the effective pressure at radius r is found to be

$$p(r) = (4\eta_s E^*/3\kappa_s^{1/2}) \int_d^\infty \{z_s - d(r)\}^{3/2} \phi(z_s)\, dz_s \tag{13.52}$$

where η_s is the asperity density N/A_0. The bulk compression w_b, which is contained in the expression for separation (13.51), is related to the effective

https://doi.org/10.1017/CBO9781139171731.014 Published online by Cambridge University Press

pressure $p(r)$ by the equations for the axi-symmetric deformation of an elastic half-space presented in §3.8. In the notation of the present section equation (3.98*a*) for the normal displacement of an axi-symmetric distribution of pressure $p(r)$ can be written:

$$w_b(r) = \frac{4}{\pi E^*} \int_0^a \frac{t}{t+r} p(t)\mathbf{K}(k)\, dt \tag{13.53}$$

where **K** is the complete elliptic integral of the first kind with argument $k = 2(rt)^{1/2}/(r+t)$. Equations (13.51), (13.52) and (13.53) have been solved by Greenwood & Tripp (1967) for a Gaussian distribution of asperity heights,

Fig. 13.11. Contact of a smooth elastic sphere with a nominally flat randomly rough surface: solid line – effective pressure distribution $p(r)$; broken line – Hertz pressure (smooth surfaces). Effective radius a^* defined by eq. (13.56).

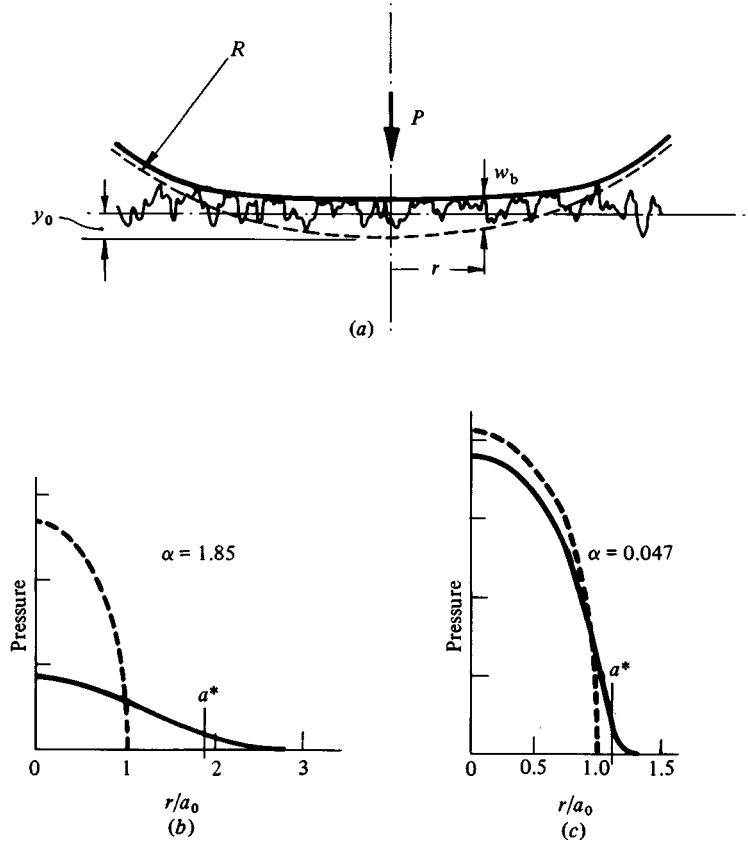

https://doi.org/10.1017/CBO9781139171731.014 Published online by Cambridge University Press

using an iterative numerical technique to find the effective pressure distribution $p(r)$.†

Effective pressure distributions, normalised by the maximum pressure p_0 and contact radius a_0 for smooth surfaces under the same load P, are plotted in Fig. 13.11(b) and (c). As expected, the effect of surface roughness is to reduce the maximum contact pressure $p(0)$ and to spread the load over an area of greater radius. The solution to equations (13.51), (13.52) and (13.53) depends upon two independent non-dimensional parameters. The first, which we shall denote by α, can be expressed variously by

$$\alpha \equiv \frac{\sigma_s}{\delta_0} = \frac{\sigma_s R}{a_0^2} = \sigma_s \left(\frac{16RE^{*2}}{9P^2} \right)^{1/3} \tag{13.54}$$

where δ_0 is the bulk compression and a_0 is the contact radius for smooth surfaces under the load P, i.e. given by the Hertz theory.‡ The second parameter is defined by Greenwood & Tripp as

$$\mu = \tfrac{8}{3}\eta_s \sigma_s (2R/\kappa_s)^{1/2} \tag{13.55}$$

which depends on the topography of the surfaces but not upon the load. The ratio of maximum effective pressure with a rough surface $p(0)$ to the maximum pressure with a smooth surface p_0 (given by Hertz) is plotted against α in Fig. 13.12 for two values of μ which bracket a wide range of practical rough surfaces. It is clear from Fig. 13.11(b) and (c) that, with a rough surface, the effective pressure falls asymptotically to zero. The contact area, therefore, is not precisely defined. One possibility is to define the 'contact' radius as the radius at which the effective pressure falls to some arbitrarily chosen small fraction of the maximum pressure. Greenwood & Tripp arbitrarily define an effective 'contact' radius a^* by

$$a^* = \frac{3\pi \int_0^\infty r p(r)\, \mathrm{d}r}{4 \int_0^\infty p(r)\, \mathrm{d}r} \tag{13.56}$$

Its value is indicated in the examples shown in Fig. 13.11(b) and (c). With this definition theoretical values of a^*/a are plotted against α for $\mu = 4$ and $\mu = 17$ in Fig. 13.13, where they are compared with experimental measurements of the

† If the elastic foundation model is used in place of equation (13.53) to find the bulk displacement w_b, together with an exponential probability of asperity heights, a solution can be obtained in closed form as shown by Johnson (1975).

‡ Greenwood & Tripp (1967) use the non-dimensional parameter $T = (8/3\sqrt{2})\alpha^{-3/2}$.

https://doi.org/10.1017/CBO9781139171731.014 Published online by Cambridge University Press

contact size. In reality the contact area has a ragged edge (see Fig. 13.14) which makes its measurement subject to uncertainty. The rather arbitrary definition of a^* is therefore not of serious consequence.

It is clear from Figs. 13.12 and 13.13 that the effect of surface roughness on the contact pressure and contact area is governed primarily by the parameter α; the parameter μ has a secondary effect. Further, we can conclude that the Hertz theory for smooth surfaces can be used with only a few per cent error provided the parameter α is less than about 0.05, i.e. provided the combined roughness of the two surfaces σ_s is less than about 5% of the bulk elastic compression δ_0.

By influencing the pressure distribution and the contact area, surface roughness influences the magnitude and position of the maximum shear stress in the solid and hence the load at which bulk yield will take place. For a smooth (Hertzian) contact the maximum shear stress has the value $0.31p_0$ at a depth $z = 0.48a$. Greenwood & Tripp find that with the pressure distributions appropriate to a rough surface, as shown in Fig. 13.11, the maximum shear stress

Fig. 13.12. Influence of surface roughness on the maximum contact pressure $p(0)$ compared with the maximum Hertz pressure p_0.

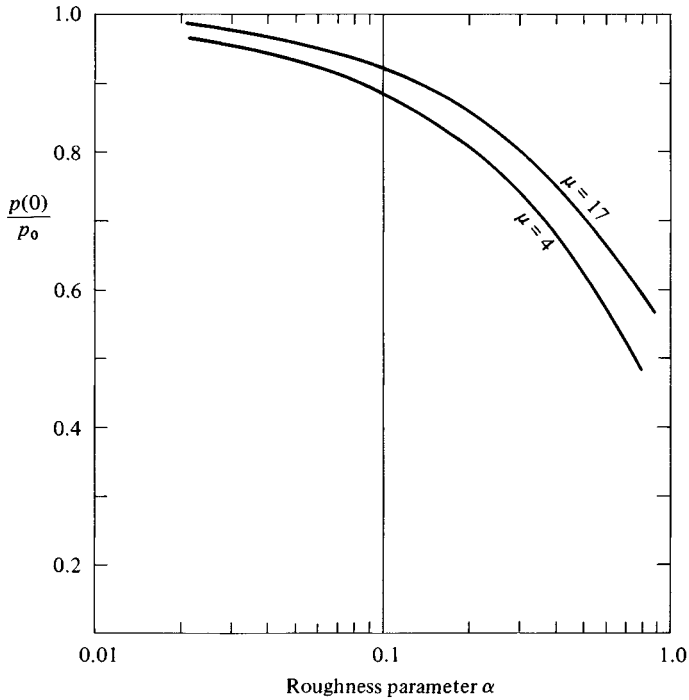

https://doi.org/10.1017/CBO9781139171731.014 Published online by Cambridge University Press

$\approx 0.29p(0)$ at a depth $z \approx 0.35a^*$. However, since $p(0)$ decreases significantly with increasing roughness (Fig. 13.12) and a^* increases (Fig. 13.13), the maximum shear stress is reduced and occurs at a greater depth than with smooth surfaces.

We now return to the question of 'functional filtering': how should the sample length and sampling interval be chosen in order to obtain appropriate values for the parameters α and μ? The sample length presents no great difficulty. Wavelengths in the surface profile which greatly exceed the nominal contact diameter are not going to influence the contact deformation appreciably, so that we should take $L < 4a_0$. Since σ is found in practice to vary approximately as $L^{1/2}$, the precise choice of L is not critical. We then use Greenwood's result (13.30) and put the standard deviation of the summit heights σ_s equal to the r.m.s. height of the surface σ measured from the profilometer trace. If the parameter α only is required no further considerations are necessary since σ is not sensitive to sampling interval. If the parameter μ is also required then values for the asperity density η_s and the asperity summit curvature $\bar{\kappa}_s$ must be determined. They are given by equations (13.31) and (13.32) in terms of the peak density η_p and the r.m.s. curvature σ_κ found from the profile trace, but both these latter quantities are strongly dependent on sampling interval. Intuitively we would expect there to be a scale of roughness below which the asperities would be immediately destroyed by plastic deformation when the surfaces were brought into contact and would not contribute significantly to the contact pressure:

Fig. 13.13. Influence of the surface roughness on the effective contact radius a^* compared with the Hertz radius a_0. Experiments: circle – $\mu = 4$; triangle – $\mu = 5$; square – $\mu = 15$.

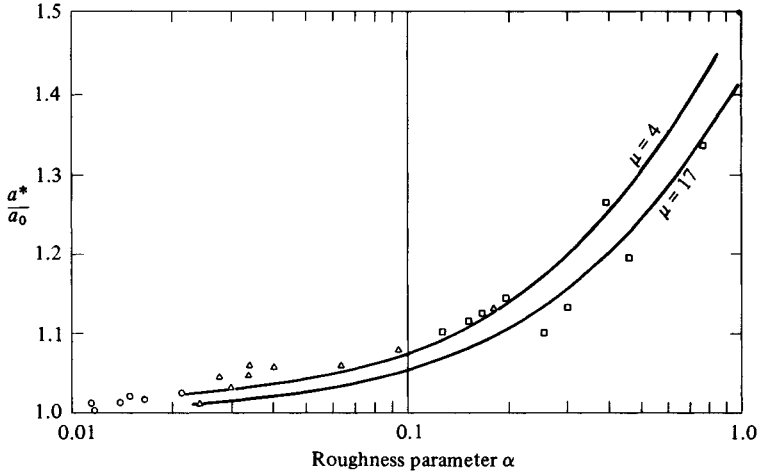

https://doi.org/10.1017/CBO9781139171731.014 Published online by Cambridge University Press

it would then be reasonable not to reduce the sampling interval below this size. However, it has proved difficult to quantify this cut-off point. At the present time most profilometers arbitrarily use a sampling interval of ~10 μm.

Tangential forces

When two bodies having rough surfaces are in contact the influence of the surface roughness upon their tangential compliance is also of interest. In rolling contact surface roughness might be expected to affect the creep coefficients.

An experimental study (O'Connor & Johnson, 1963) of a hard steel smooth sphere, pressed into contact with a rough flat by a constant normal force, showed

Fig. 13.14. Contact of a smooth steel ball, diameter 25.4 mm, with a rough steel flat: (*a*) $\sigma = 0.19$ μm, $P = 10$ kg, $\alpha = 0.043$; (*b*) $\sigma = 0.54$ μm, $P = 60$ kg, $\alpha = 0.043$; (*c*) $\sigma = 0.54$ μm, $P = 4$ kg, $\alpha = 0.22$; (*d*) $\sigma = 2.4$ μm, $P = 40$ kg, $\alpha = 0.22$.

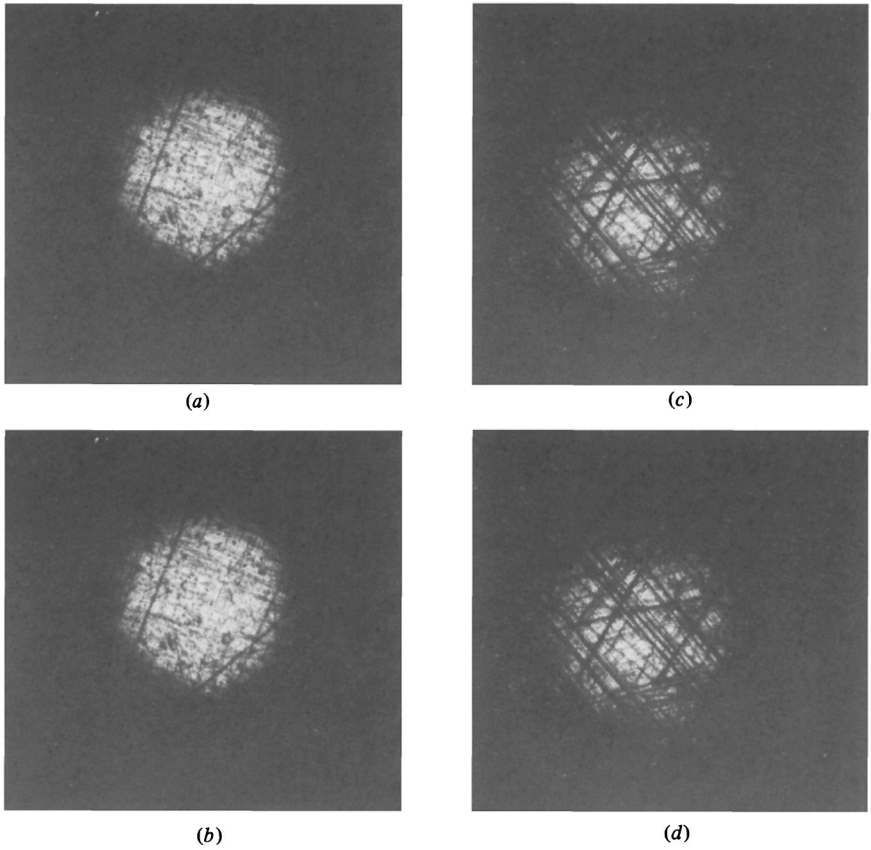

(*a*) (*c*)

(*b*) (*d*)

https://doi.org/10.1017/CBO9781139171731.014 Published online by Cambridge University Press

that the compliance under the action of a superimposed tangential force, given by equation (7.42), was affected very little by the roughness of the surface. This was the case from the start with a rough ground hard steel surface in which the asperity deformation was predominantly elastic. With a scratched surface of soft steel, in which the asperity deformation was fully plastic, the tangential compliance was somewhat greater on first load than that given by equation (7.42) for smooth elastic surfaces, but was close to equation (7.42) on subsequent loadings. The small effect of roughness on tangential compliance can be explained as follows. First, the tangential elastic compliance of an individual asperity is comparable with its normal compliance as demonstrated by equations (7.43) and (7.44), provided that the ratio of the tangential to the normal traction is relatively small compared with the coefficient of limiting friction. In the central region of the contact area, as Fig. 7.7 shows, the tangential traction is a minimum while the normal pressure is a maximum. The real contact area in this region will be high and, in consequence, the compliance of the asperities will be small. Since the tangential traction is also small in that region the contribution of the asperity deformation to the bulk compliance is negligible. At the edges of the contact when the tangential traction is larger and the normal pressure smaller, some micro-slip will take place in the same manner as described in §7.2(*d*).

In rolling contact, the creep ratio ξ is determined by the strains in the region of no slip at the leading edge of the contact area. In this region the tangential traction is less than the normal pressure so the same argument applies, though with less force, to explain the small influence of surface roughness on creep in rolling contact.

The parameter α, which was used as a measure of the effect of surface roughness on static contact under a purely normal load should also apply to static and rolling contacts under the action of tangential loads. However the condition that $\alpha < 0.05$ for the effect of surface roughness to be negligible in normal contacts is likely to be somewhat conservative when applied to tangential forces.